Local cathodoluminescence and its capabilities for the study of band structure in solids

G. V. Spivak, V. I. Petrov, and M. K. Antoshin

M. V. Lomonosov State University, Moscow

Usp. Fiz. Nauk **148**, 689–717 (April 1986)

A review of the applications of the scanning electron microscope cathodoluminescent mode is given. Particular attention is devoted to the kind of information that can be obtained by modifying the method in different ways, the problems of spatial resolution and the formation of image contrasts. Results obtained for GaAs, GaP and other optoelectronic materials show the advantages of the local cathodoluminescence method in determining local values of electrophysical parameters in multilayer epitaxial structures, distribution of optically active impurities, etc. These features make the method uniquely useful for the growth of optoelectronic structures with prescribed properties.

TABLE OF CONTENTS

1. INTRODUCTION

The phenomenon of cathodoluminescence (CL)—the emission of light in the ultraviolet, visible and infrared areas of the spectrum as a result of irradiation by electrons—has been known for a long time. Initial interest in this subject was related to the study and use of phosphors. While addressing the practical problem of developing the best possible coating for the screens of cathode-ray tubes, researchers investigated the radiative recombination processes and details of the band structures of II-VI semiconductor compounds. As for the cathodoluminescence method itself, it has come to be a standard tool in the study of band structure in solids (mainly for the energy levels participating in processes of radiative recombination), along with other methods as photoluminescence, optical absorption and reflection of light.

Recently, interest in cathodoluminescence has increased significantly in connection with the rapid development of optoelectronics. The fabrication of high efficiency semiconductor lasers and LED's, which are multilayer structures with layer thicknesses of several or tens of microns, called for the development of new techniques with high spatial resolution which could create predetermined distribution of radiative recombination centers within these layers by controlled introduction of active impurities during the growth process. Scanning electron microscopy has opened up many possibilities in this area.

The operating principle of a scanning electron microscope (SEM) is as follows: a sharply-focused electron beam (down to 2–5 nm in the best SEM models) is scanned by deflecting coils, tracing on the surface of a sample a pattern similar to a television raster (Fig. 1). The interaction of electrons in the primary beam with the object give rise to a number of phenomena—secondary electron emission, characteristic x-ray emission, cathodoluminescence and others. Each of these phenomena can be used to modulate the intensity on the screen of a cathode-ray tube included in a receiver circuit. A second electron beam is scanned across this screen simultaneously and in phase with the electron beam scanning across the sample. By studying SEM images from various signals one can obtain a great deal of information with minimum sample requirements. For example, when emission of secondary electrons is used, one can obtain information about surface topography and distribution of electric and magnetic fields; when reflected electrons are used information about the composition of the object and finally when the self-focusing effect of the primary electron beam is used, information about crystal structure of the object. If an electron, x-ray or optical spectrometer is added to the SEM sam-

 0038-5670/86/040364-17$01.80

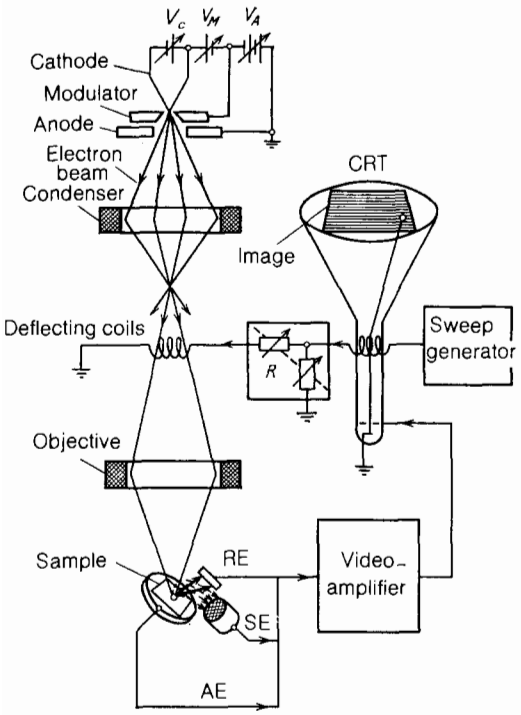

FIG. 1. A schematic showing the operating principle of the scanning electron microscope: CRT—cathode-ray tube; RE—reflected electrons; SE—secondary electrons, AE—absorbed electrons.

ple chamber, it is possible to analyze spectroscopically the composition of materials in any small area of a sample by focusing the electron beam on that area using the image[1]. This "point by point" way of using cathodoluminescence, referred to as the local cathodoluminescence method, makes it possible to study the structure of energy levels in small areas of a sample.

The resolution or, as it is also commonly called, the point to point resolution, is not the same for the various SEM modes; it is determined by the nature of the sample and the distinctive characteristics of the phenomena which give rise to the signal used to form the image. In SEM work it is customary to indicate the secondary electron resolution, which is the best achievable resolution and which coincides with the size of the electron beam on the sample. The resolution in the cathodoluminescent SEM mode is significantly worse for three reasons:

1) Unlike the secondary-electron emission mode, where the maximum resolution is achieved for small electron-beam currents (10^{-11} A), the cathodoluminescence mode requires currents 10^{-7}–10^{-9} A because of the small signal amplitude, especially for objects with small radiative recombination efficiency; this entails an increase in the cross section of the electron beam up to fractions of a micron.

2) Further, when secondary electron emission is used, the size of the region with a high density of secondary electron emission, which determines the resolution, coincides with the size of the electron beam on the sample because of the small geometrical escape depth of secondary electrons. In the cathodoluminescence mode, the emission originates deep in the sample, where the primary beam has already undergone strong scattering, and the size of the area of intense luminescence is significantly larger than the size of the beam at the sample surface. Obviously, for very thin free-standing films this negative factor is irrelevant.

3) In the cathodoluminescence mode the resolution is also degraded because of diffusion of electron-hole pairs generated by the electron beam, whose recombination leads to emission of light. In materials with a large minority carrier diffusion length this can lead to significant loss of resolution, which sometimes can be partially removed by using SEM in the stroboscope regime or by processing the signal on a computer.

As a result of all these factors the spatial resolution in the cathodoluminescence mode can vary over a wide range from several nanometers up to several microns.

The local cathodoluminescence method is used widely for investigation of various kinds of samples, including geological and even biological samples. For example, when applied the geological samples, the local CL method has led to determination of the phase composition of volcanic glass[2], samples of soil[3], clays[4,5] and lunar regolith.[6] A detailed review of the study of geological samples by local cathodoluminescence method has been published.[7]

Despite the fact that attempts were made to use the CL SEM mode for the study of biological samples in the early days of development of scanning electron microscopy[8], the CL mode has been properly developed as a tool in medico-biological research only during recent years.[9] The problem is that many biological samples have relatively weak CL efficiency, and when the signal is increased by increasing the probe current, the fragile biological structures are sometimes destroyed. Nevertheless, one should note definite advantages of CL method compared to traditional fluorescent microscopy: much larger depth of field, better resolution and the possibility of combining it with other SEM modes, for example with x-ray microanalysis.

There are two ways to study medico-biological samples with CL: observation of "natural" CL from the studied object, and study of a stained sample, i.e., a sample containing some solution of a substance which exhibits strong luminescence when irradiated by an electron beam; the sample is studied by examining the area where this substance accumulates. For example, localization of herbicides in the leaves of plants or calcified areas in human aortas have been studied by the first method, while passage of substances through the root channels of plants has been studied by the second method.

It is characteristic of medico-biological samples that modern methods of preparing them (i.e., fixation with the help of various alcohols or of osmium tetroxide, fast freezing, drying at some critical temperature in an inert gas atmosphere, etc.), often lead to preservation only of the surface geometry of a sample, and not of its internal structure and composition. This situation has always led to attempts to study biological samples in wet form.[10] The possibility of such studies using the CL mode had been demonstrated in Ref. 11. Samples were attached to the photocathode of a photomultiplier that was placed in a chamber isolated from

the vacuum pumped area of the microscope and having an autonomous pumping system which could provide any desired pressure (up to one atmosphere). An electron beam reached a sample through a 0.5 mm hole covered by a thin polymer film.

As mentioned above, the local CL method offers the most diversity as to samples studied. To the list of samples given above could be added metals (Lilienfield's emission)[12], polymer and synthetic materials and fibers[13], rocket fuel[14], threadlike single crystals[15] and many others. This article will summarize and discuss the capabilities and prospects of local cathodoluminescence SEM methods, using as an example the study of physical samples—semiconductors and dielectrics. A number of previous review articles and bibliographies are given in Refs. 16,17.

2. INTERACTION OF ELECTRONS WITH SOLIDS

When an electron beam penetrates a sample its electrons interact with the atoms and electrons of the sample and are scattered. This scattering can be of two types: elastic scattering, when the electron energy is practically unchanged, but the direction of the electron's motion can be significantly altered, and inelastic scattering when the electron energy decreases because part of this energy is transferred to atoms and electrons of the sample, while the direction of the electron motion changes only insignificantly. In practice, both elastic and inelastic scattering occur; inelastic scattering is more probable, however, for elements with low atomic numbers, and elastic scattering is more probable for elements with high atomic numbers. It is the inelastic interactions in a sample that cause the secondary phenomena used in SEM to obtain information about an object: secondary electron emission, cathodoluminescence, etc. Despite the fact that during elastic electron interactions no energy is transferred to a sample, they play a very important role; it is these interactions that cause the "spreading" of the primary electron beam as it penetrates a sample, and the formation of so-called energy dissipation areas and generation of various signals. The size of the area depends on the energy of the electron beam, the composition of the sample and the ionization energy for the particular ionization process whose signal is being used in SEM to obtain the information about the sample; this size can significantly exceed the size of the beam at the sample. The shape of this area depends on the atomic number of the material of the sample: for materials with a low atomic number it is an elongated pearlike shape, for materials with a high atomic number it is, because of strong elastic interactions, closer to a truncated sphere. The Bethe formula is often used to estimate the penetration depth of electrons into a sample. This formula gives the dependence of the energy loss dE by an electron over an element of trajectory ds as a function of sample parameters and energy E of the electron:

$$\frac{dE}{ds} = -\frac{2\pi e^4 N_0 Z\rho}{AE} \ln \frac{1{,}166E}{J}, \qquad (1)$$

where N_0 is Avogadro's number, Z is the atomic number, A is the atomic weight, ρ is the density, J is the average ionization potential of an atom, and e is the electron charge. Integrating the expression ds/dE from the initial energy to zero gives the average distance traversed by an electron along its trajectory in a solid. Since the real trajectories are broken lines because of elastic collisions and deviate strongly from a straight line, the penetration depth calculated in this way will be an overestimate, especially for materials with high atomic numbers. Still, this penetration depth can be used for a rough estimate of not only the maximal depth, but also the width of the energy dissipation area for primary electrons in SEM.

In semiconductors and dielectrics a significant part of the energy deposited by the primary electrons of a beam is used to form nonequilibrium electron-hole pairs. When these pairs recombine, energy is released in the form of cathodoluminescence (for radiative recombination) or in the form of phonons (for radiationless recombination). After being generated in the energy dissipation area for primary electrons, electron-hole pairs diffuse into adjacent regions of the sample. The distribution of nonequilibrium carriers in a sample can be found from the solution of the diffusion equation. For semiconductors with a very small radiative recombination efficiency (re-emission is absent), and for low levels of excitation this equation has the form

$$D\nabla^2(\Delta n) - \frac{\Delta n}{\tau} + g(r) = \frac{\partial(\Delta n)}{\partial t}, \qquad (2)$$

where Δn is the density of nonequilibrium carriers, D and τ are the diffusion coefficient and lifetime and $g(r)$ is the generation rate of carriers by external excitation. For the particular case of a point source of nonequilibrium carriers the stationary solution of equation (2) has the form:

$$\Delta n = \frac{Ae^{-r/L}}{r}, \qquad (3)$$

where $L = (D\tau)^{1/2}$ is the diffusion length for minority carriers.

In the case when the radiative recombination efficiency is high (i.e., the internal quantum efficiency is close to one), one must add another term to equation (2) describing the generation of minority carriers by re-absorption of recombination radiation.

Cathodoluminescent radiation originates from an area of the sample that has nonequilibrium charge carriers ($\Delta n \neq 0$). The efficiency of cathodoluminescence, i.e., the fraction of nonequilibrium charge carriers which recombine radiatively, depends on the nature of the sample as well as on the level of excitation. Radiative recombination in semiconductors and dielectrics can originate from several processes: band-to-band transitions, band-to-impurity level transitions and the decay of a free or bound exciton. Nonradiative recombination also can occur in several different ways. For a number of materials collision-induced recombination (Auger processes) begins to play a major role at very high levels of excitation. As the excitation level increases further, irreversible changes in the material properties can take place because of local heating.

Usually the processes of radiative and nonradiative re-

combination take place simultaneously in luminescent materials. The probability of recombination is equal to the sum of probabilities for all types of recombination:

$$\frac{1}{\tau}=\frac{1}{\tau_r}+\frac{1}{\tau_1}+\frac{1}{\tau_2}+\cdots, \quad (4)$$

where τ is the average lifetime of minority carriers, τ_r is the lifetime of radiative recombination and τ_i is the lifetime of individual nonradiative processes. The intensity of the CL signal depends on this average lifetime and is determined both by radiative and nonradiative processes. This complicates to some degree the interpretation of image contrasts for this mode.

3. RESOLUTION AND IMAGE CONTRAST IN THE CATHODOLUMINESCENT SEM MODE

As was said earlier, resolution in the cathodoluminescent SEM mode depends not so much on the size of the primary electron beam cross section at the object as on the size of the area within which electron-hole pairs are generated and then diffuse across. In materials with high quantum efficiency the size of the actual region where pairs are generated can substantially exceed the size of the region where pairs are initially generated by the electron beam, because of "photon transport"[18]. By this we mean the excitation of nonequilibrium charge carriers by reabsorption followed by their reemission as intrinsic recombination radiation. As a result of this absorption-emission sequence an electron-hole pair "moves" in the sample a distance equal to the distance traversed by a photon. In the absence of reemission the area where pairs are generated practically coincides with the energy dissipation area for primary electrons and any additional movement of pairs takes place by diffusion. For substantial diffusion lengths the size of the area occupied by injected carriers can significantly exceed the cross section of the primary electron beam on the sample. For example, for a beam with a cross section of 1 μm and for a diffusion length of 3 μm the size of that area is about 7 μm. For an average energy of pair formation of 3 eV, an electron beam with an energy of 30 keV and a current of 10^{-6} A creates about $6\cdot10^{16}$ pairs/sec in a volume of $2\cdot10^{-9}$ cm^3. For the minority carriers lifetime of 10^{-9} sec the average density of excess carriers is $3\cdot10^{16}$ cm^{-3}. In materials with large lifetimes, even higher densities of excess carriers can be achieved.

The density distribution of excess carriers in the area where they are present is far from uniform. Naturally, the resolution is determined by that portion of the area where the density of excess carriers is large. Due to the small number of recombination events CL radiation from regions with low carrier density cannot carry useful information about details of those regions and serves as a background for the main CL signal from regions with high carrier density. The resolution may also be influenced by the presence in the sample of layers with low efficiency of radiative recombination and of surface films, and by the value of the refractive index of the sample, the sample's absorption coefficient, etc.

The background signal from areas with low carrier density can be eliminated, thus effectively limiting the geometrical dimensions of the radiating area and increasing spatial resolution in the CL mode. This was done in the case of pulse irradiation of a sample in SEM by limiting the information collection time to values significantly smaller than lifetime of minority carriers. In this case the microscope operates in the stroboscopic mode, and the CL signal is recorded only at the very beginning of the carrier diffusion process when the stationary distribution has not yet been established, so that the size of the nonstationary distribution is significantly smaller than the size of the stationary distribution.[19] Naturally, this approach will be effective if the diffusion length significantly exceeds the size of the region where pairs are generated. A disadvantage to this pulsed regime is the decrease in the useful signal which occurs simultaneously with elimination of the background signal; therefore, in order to receive images of good quality, one should significantly increase the accumulation time of a signal, i.e., the exposure time.

The resolution can also be increased by processing the images on a computer. In this case one must assume *a priori* a model that quantitatively describes the minority carrier distribution function in a sample. Such a function can be derived from a correct solution to equation (2). The origin of the increase in spatial resolution is the same in both cases—deletion of part of the signal which forms the image. Thus, in order to check the theoretical model, it is recommended to compare images received by both methods, since the stroboscope method does not depend on any *a priori* considerations.

In general, all such methods of signal processing allow one to separate out only those variations of signal that exist in the signal before its processing, although these variations may be difficult to distinguish. From this point of view a significant increase in exposure, i.e., accumulation of signal with subsequent digitization of brightness values will allow one to register weak variations of signal on the large background noise and will thus contribute to the increase of image resolution.

The image contrast in the CL SEM mode is determined by the changes of CL characteristics from one point of the sample to another; these changes depend on the variation of local values of the sample parameters or characteristics. By sample characteristics we mean everything that causes changes in the energy band structure and in the concentration of recombination centers: composition, level of doping, presence or absence of certain radiative and nonradiative recombination centers, crystal structure, degree of strain, presence of structural defects and temperature. The variable characteristics of CL which can be used to represent information depending on the system of CL recording, are integrated intensity, spectral composition, kinetics of rise or decay of luminescence for pulsed irradiation and polarization of CL radiation. Apart from these causes, local CL characteristics can be influenced by the presence of surface films on the sample that can absorb and reflect recombination radiation, and the topography of the surface of the sample, as, for example, in the case of phosphors, which are powders composed of small randomly-oriented crystals.

The dependence of the CL intensity on doping[20] and

excitation levels has been studied experimentally in single GaAs crystals. It has been shown that for a given sample temperature the CL efficiency goes through a maximum as a function of doping concentration (Fig. 2). By studying this doping dependence of the CL efficiency, one can correctly explain the contrasts on CL images. For example, when impurity segregation takes place on dislocations, the dislocation images in the CL mode are lighter or darker relative to the background, depending on which side of the maximum in the curve shown in Fig. 2 the point which corresponds to the initial doping concentration lies (i.e., on the increasing or decreasing side).

The sensitivity of the CL SEM method to the presence of small amounts of luminescing impurities in the sample is rather high compared with other methods of material analysis (x-ray microanalysis, laser microanalysis, Auger spectroscopy, etc.) and is 10^{-7} percent or 10^{-18} g.[21]

The presence of structural defects that usually give rise to deep energy levels and act as centers of nonradiative recombination leads to a decrease in the CL intensity; this fact, as will be shown later, is used to make them visible. For example, in AlGaAs–$In_x Ga_{1-x} As$ structures both the lattice mismatch and dark-line density (i.e., the images of mismatch dislocations in the CL mode) near the heterojunction increase with increasing x.[22] In some cases, however, structural defects can contribute to radiative recombination. For example, in single-crystal samples of MgO, strain-induced point defects near dislocations can cause an increase in the CL intensity from the compressed areas, while dislocations formed during growth have no point defects and consequently have no such influence on the CL. These areas also exhibit a different kind of CL intensity variation when irradiated by an electron beam: under electron-beam irradiation the intensity decreases with time from strained areas and increases from unstrained areas. It is possible that the difference in CL behavior of the strained areas is caused by the presence of negative ion vacancies. Other effects induced by electron irradiation are due to changes in color centers.[23] A similar increase in the CL intensity from dislocations has been observed in single-crystal samples of YAG–$Y_3Al_5O_{12}$ due to the clustering of luminescent ions and oxygen vacancies near dislocations.[24] In GaAlP the red CL emission band due to defects formed during growth originates in the strained area near the heterojunction (Fig. 3).[25]

From all that was said above concerning the influence of structural defects on CL, it is clear that the CL is strongly affected by their presence. It follows from this that the CL SEM mode can be successfully used to control the crystal quality of semiconductor layers, and thereby increase the efficiency of semiconductor devices made from such layers; this is especially important for heterojunction devices.[26]

With a decrease of sample temperature the recombination radiation intensity increases sharply. This is due to a decrease in the number of nonradiative transitions at low temperatures. Thus, the use of liquid nitrogen and especially liquid helium temperatures provides an opportunity to study luminescence in materials with small intrinsic quantum efficiency. The temperature dependence of the CL intensity has been used to determine the local temperature in GaAs Gunn diodes during their operation. The accuracy to which the local temperature was measured was $\pm 4°$ at a spatial resolution of $\sim 1\,\mu$m.[27]

The CL emission spectra depend strongly on sample composition. For example, a variation in ternary alloy composition leads to a change in the forbidden gap energy E_g and to a shift in the absorption edge; the position of the edge corresponds uniquely to a particular composition. This fact is often used to determine the alloy composition from a calibration curve previously obtained, e.g., the work on $CdS_{1-x}Se_x$ alloys in Ref. 28.

When several radiative recombination mechanisms are operating, the CL spectrum can depend strongly on the concentration of one of the activators; for example, on the concentration of nitrogen in gallium phosphide (Fig. 4).[29] In this case, in addition to a "redistribution" of the recombination among the various recombination channels (i.e., the relative contribution of each channel to the recombination is

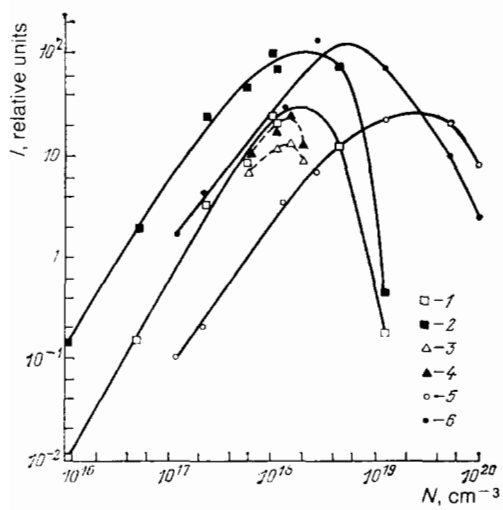

FIG. 2. Dependence of relative intensity I of the edge CL in a GaAs single crystal on the doping concentration (N).[20] For the n-type: 1, 2—Te, Se; 3, 4—Sn; for the p-type; 5, 6—Cd, Zn. 1, 3, 5 correspond to temperature of 300 K; 2, 4, 6—to temperature of 77 K.

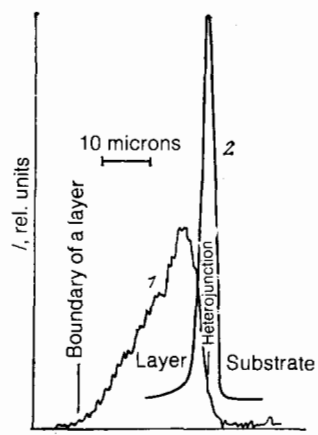

FIG. 3. Intensity distribution of the red CL band with $h\nu_{max} = 1.94$ eV[1] and the induced type signal (2) from the cleaved surface of a $Ga_{0.5}Al_{0.5}P$ structure.[25]

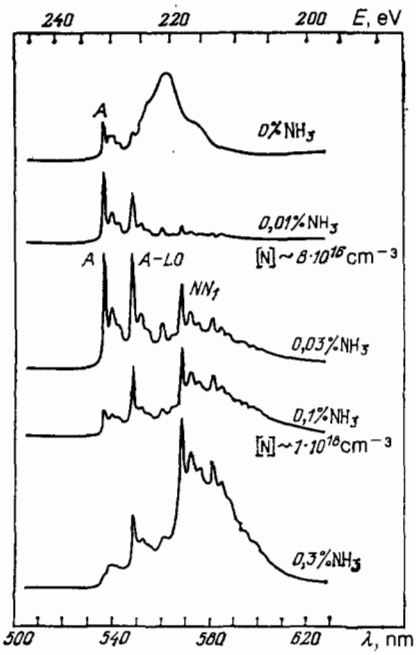

FIG. 4. CL spectra of p-GaP : N layers with concentration of carriers $5 \cdot 10^{17}$ cm^{-3} for 80 K and various doping concentration of nitrogen.[29]

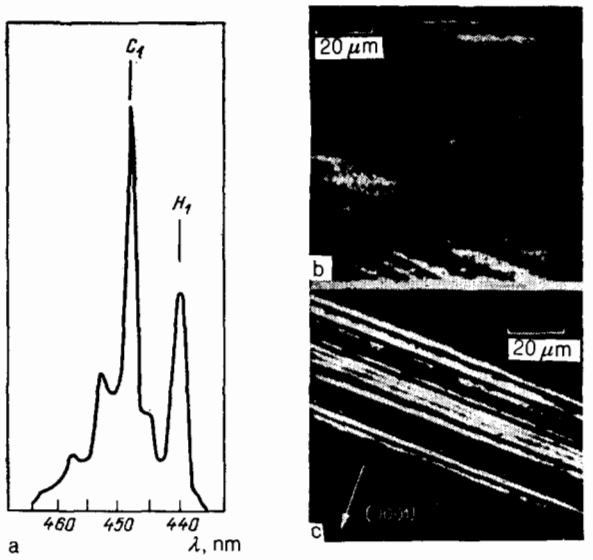

FIG. 5. CL spectrum of a epitaxial ZnSe layer (a) and a monochromatic CL microphotograph of the same area obtained by using the peak H_1, corresponding to recombination of the exciton bound to defects in the hexagonal phase (b), and by using the peak C_1, corresponding to recombination of exciton bound to defects in the cubic phase (c) ($T = 77$ K).[30]

changed, along with the corresponding intensity in that portion of the spectrum fed by the channel), the luminescent intensity due to bound excitons on individual nitrogen atoms (line A) is also changed because of self-absorption of these nitrogen atoms.

By using a monochromator to select various spectral regions which correspond to a particular radiative recombination mechanism, and using the resulting signal to construct the image (a so-called monochromatic CL image), one can determine in which area of the sample a given mechanism is active. For example, using the fact that emission from the hexagonal and cubic phases of ZnSe occurs in different parts of the spectrum, identification of these phases has been carried out with the help of monochromatic CL images (Fig. 5).[30]

Sometimes for various reasons the CL spectral variations are so small that they cannot be determined from the spectra themselves. In other cases, the sample areas that emit CL of various spectral compositions are randomly distributed across the sample and cannot be distinguished in the integrated CL or in any other SEM mode. In these cases it is convenient to pursue the analogy between regular color fluorescent microscopy and the CL color mode in SEM, i.e., to record the CL color images directly in natural light on the screen of a color projector. Because of the high sensitivity of the eye to color, it is possible to distinguish very small changes in the CL spectrum on the color image. This method can also be used for phase analysis. For example, the sharp difference in color between scheelite (light blue) and molybdoscheelite (yellow) allows one to discriminate between these phases and to study zonality and replacement of rock molybdoscheelite in rock forms.[31] The mechanism of small-crater formation during cumulative loading of MgO has been studied using the CL color mode.[32] The appearance of areas with a different luminescence color in the vicinity of the area under pressure is visible in color images; at the same time no changes in the picture are seen in the usual CL mode. The high sensitivity of the human eye to color variation can also be used to increase the amount of information contained in the image by using color coding.[33]

The dynamics of spectral variation with temperature has been studied for samples of lunar soil and gallium phosphide p-n junctions. In order to make accurate temperature measurements under the beam one can use the known temperature dependences of edge emission and exciton recombination peaks. In indirect-gap band structures, where several recombination mechanisms may exist, the recombination mechanism itself can change with temperature, and so this temperature measurement method can not be used. This is the case, for example, in GaP, where because of changes in the recombination mechanism there is no noticeable peak shift in the CL emission from the p-region.[34]

Details of CL kinetics are studied using the microscope in the pulsed mode. In this mode one can study the CL rise and decay kinetics and by using the stroboscopic method, observe the CL distribution images across the sample for various phases of the dynamic processes. In this latter case one can detect inhomogeneity of the kinetic processes taking place in various areas of the sample and, in particular, the process of trap filling.[35] Using this method, the CL relaxation times in GaP[36] and in activated Mn^{2+} phosphors[37] were analyzed; in addition, a propagating acoustic wave was made visible in single crystals of quartz.[38] The problem of measuring carrier lifetimes in semiconductors from the decay of the CL signal with pulsed excitation has been studied in detail in Ref. 39, where it was shown how surface recombination, self-absorption and the finite size of the sample can affect the CL decay. Theoretical calculations using a simplified model of the carrier generation function have demon-

strated that under certain conditions one can determine actual carrier lifetimes and surface recombination rates from the temporal behavior of CL decay for pulsed excitation. A method which allows one to obtain maps of local lifetime distributions over the sample has been suggested in Ref. 40; in Ref. 41 this method was modified with the use of color coding. The use of color cathodoluminescence enables one to observe the local kinetics of CL spectra across an entire sample. Such observations have been carried out on samples of molybdoscheelite and single-crystal semiconductor samples.[42–46] Evidently, the dynamic CL spectra of various phases of luminescence relaxation processes can also be recorded in the stroboscopic mode by passing the CL emission through a monochromator,[45,46] but the use of color CL is not only more convenient, but is also more sensitive to small variations in spectral composition, although in practice the information so obtained is only of a qualitative character. In the stroboscopic mode differences in the kinetics between various phases of the sample can be used to identify these phases even when their emission has very similar spectral composition. For example, SEM has been used to solve the structural problem of finding inclusions of different phases in the bulk of a heterogeneous crystal and to study processes of energy migration in doubly activated phosphor crystals.[42,45,46] Figure 6 shows two photos of molybdoscheelite samples, for continuous irradiation by electrons (on the left) and for pulsed irradiation (on the right). Since the risetime of luminescence in scheelite is two times shorter than the risetime in powellite, one has an opportunity to observe with high resolution the decay process in molybdoscheelite samples in which segregation of the powellite phase has occurred. It should be noted that the proposed method can be considered as an artificial confinement of the emission region, giving improved spatial resolution in a continuous sample. Besides, "waiting" for luminescence radiation to decay can be a useful feature in the study of dielectrics (scintillators, biological samples, minerals, etc.), which are susceptible to charging by electron irradiation. In these cases a charge generated by the electron beam has enough time to dissipate because of the intervals between periods of irradiation by the electron probe.

Recording of radiation already in the initial stage of its rise makes it possible to record also the local CL spectra with high spatial resolution in materials with sufficiently large quantum efficiency.

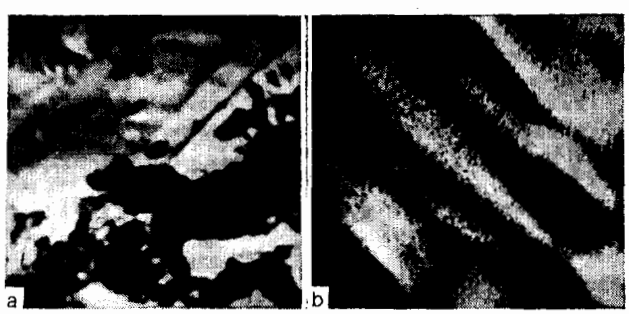

FIG. 6. Microphotograph of molybdosheelite in CL regime for continuous (on the left) and pulsed (on the right) radiation (magnification in picture on the right is 4 times larger).

CL kinetics, like CL intensity and spectral composition, depends not only on the composition of the sample and the presence of various recombination centers, but also on the conditions of the experiment, particularly on temperature. In Ref. 47 this fact was used for temperature measurements. For this purpose a calibration curve describing the dependence of the CL rise rate as a function of sample temperature was plotted for ZnSe samples; this made it possible to measure the local temperature of such samples, provided, of course, that the sample is sufficiently uniform.

First attempts to measure the polarization of CL radiation in the case of local irradiation by an electron beam were made in Refs. 48–50. Crystals of natural willemite activated by Mn^{2+},[48] sphalerite and molybdoscheelite, were investigated, along with artificially grown barium titanate and KDP[49], and both natural and synthetic diamonds.[50] The image contrast depends on the orientation of the electromagnetic field vectors. CL radiation was recorded with two photomultipliers, in front of which were placed two polarizing color filters with mutually perpendicular orientations through which radiation was passed.[49] Signals from the photomultipliers were amplified and sent alternately to a microscope videocontrol, which made it possible to obtain CL images for two different orientations of the electromagnetic field vectors, to compare them, carry out measurements of polarization and, using color coding, to obtain images carrying information about the polarization distribution over the sample.

4. EXPERIMENTAL TECHNIQUE

The first work on local cathodoluminescence was carried out using x-ray microanalyzers. A visible light microscope attached to the sample chamber was used to collect the CL radiation (Fig. 7a). Recording was done with a photomultiplier placed immediately after the exit port of a visible light microscope (integrated CL), or after the radiation had passed through a monochromator (spectral CL). If, in addition to mirrors, the prisms and lenses of the light microscope were used[51], the transmitted radiation was limited to the visible part of the spectrum. Integrated CL can be recorded by placing a light fiber connected to a photomultiplier, or simply the photodetectors themselves, in the immediate proximity of the sample. CL radiation from low efficiency GdTe and Si samples was detected with Ge and PbS solid state photodetectors placed in this way.[52,53] Photodetectors can be also placed under the sample if it is sufficiently thin. In this case a "transmission" CL method is being used, which enables one to observe structural effects in the bulk of a material.[54] Another method of extracting CL radiation from a sample chamber is the use of a parabolic mirror and a focused lens[55] (Fig. 7b). The collection efficiency of CL radiation for such a system can approach 95%. Systems using mirrors and lenses are complicated to align; however, unlike systems with flexible light fibers (for example, an elliptical mirror with a sample placed at one focus and the tip of the fiber which conducts away the radiation, placed at the other focus (Fig. 7b)[12], these optical trains allow one to convey radiation in an optimal way to the slit of a monochromator,

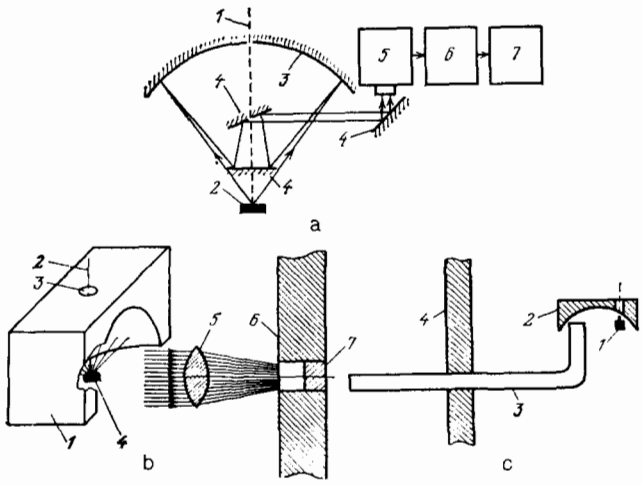

FIG. 7. Experimental apparatus for collection and extraction of CL radiation. a) by using a visible light microscope; 1—current probe, 2—sample, 3—spherical mirror, 4—flat mirror, 5—photomultiplier, 6—amplifier, 7—recording device[51,59], b) by using a parabolic mirror; 1—paraboloid mirror, 2—current probe, 3—beam aperture, 4—sample, 5—lens, 6—wall of the sample chamber, 7—exit window,[55] c) by using an elliptical mirror; 1—sample, 2—ellipsoid mirror, 3—optical fiber, 4—wall of the sample chamber[12].

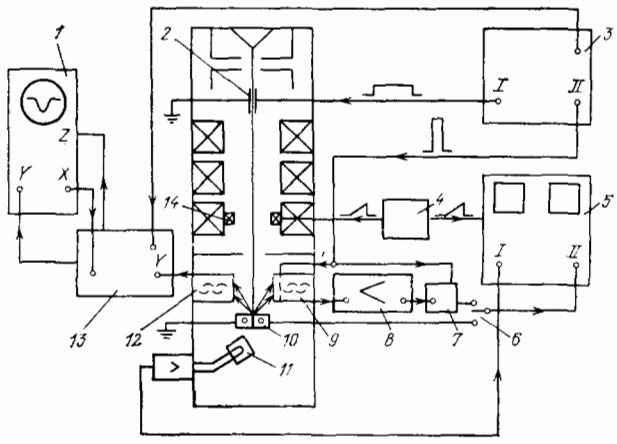

FIG. 8. Block-diagram of a stroboscopic SEM for studying time-dependent CL processes. 1—oscilloscope; 2—SEM column deflecting plates; 3—pulse generator; 4—sweep generator block; 5—videocontrol system; 6—mode switch; 7—synchroselector; 8—tuned amplifier; 9—photomultiplier with strobing shutter; 10—sample; 11—secondary electron collector; 12—fast response photomultiplier; 13—stroboscopic attachment.

utilizing its angular aperture to the fullest extent.

Recording spectra with monochromators usually takes place sequentially across the spectral range. The use of optical multichannel analyzers (OMA) has made possible the conversion from sequential accumulation of information to simultaneous accumulation across the entire spectral range or across all time intervals of the CL relaxation pulses. In both cases, spectral or temporal dispersion of radiation is transformed into spatial dispersion (in the first case with the help of a monochromator with a remotely placed exit slit, in the second case with the help of a streak camera); then this spatial picture is read simultaneously by optical multichannel analyzers whose output is accumulated in the various analyzer channels.[56,57] This makes it possible to reduce substantially the information recording time and to exclude the influence of instabilities during system operation which can be quite significant for prolonged times involved in sequential recording.

One should note separately the use in SEM of a new method of spectral recording with an improved signal-to-noise ratio that is especially important for infrared spectral recording.[58] The authors use Fourier spectroscopy, i.e., they record interferograms of CL radiation, from which they obtain the optical spectrum by Fourier transformation. The installation was specially developed for CL studies. Its distinct features are: 1) horizontal location of a column for better interface with optical devices, whose optical axes are usually horizontal; 2) the possibility of achieving beam currents of 40 μA for a spot size of 0.5–4 μm. CL relaxation processes in silicon have been studied using this apparatus.

The stroboscopic SEM mode described above was used to record CL kinetics in the system whose block diagram is shown in Fig. 8. In this case an electron beam was modulated by an electronic shutter made of a pair of deflecting plates and a diaphragm, and the pulsed CL was registered in two ways. In the first case, in order to obtain stroboscopic images of the sequential radiation decay across the sample, a signal from a strobed photomultiplier was sent after synchronous detection to a microscope videocontrol system. The opening of the photomultiplier (and therefore the recording) was implemented by pulses from the second channel of the same generator, delayed in relation to the first channel. As a result one obtains images of various stages of the luminescence decay some regulated time after irradiation by the electron beam. In order to obtain quantitative information, the radiation was recorded using another photomultiplier, whose signal was observed with the help of a stroboscope oscilloscope.

5. INVESTIGATIONS OF SEMICONDUCTOR MATERIALS AND DIELECTRICS

5.1. III-V compounds and ternary compounds based on them

GaAs. The first detailed SEM study of luminescent semiconductor materials was done on tellurium-doped single crystals of GaAs.[59] GaAs is a direct gap material with high quantum efficiency whose emission spectrum is in the near infrared between 0.7 to 1.2 μm. Images in the CL mode reveal black and white stripes related to variations in the Te concentration which appears in the sample during the growth process. More detailed studies of GaAs doping inhomogeneities were done using devices having attachments for luminescence spectral analysis. A method for determining the doping concentration of Te-doped gallium arsenide was developed in Ref. 60. The dependences of the CL peak energy position and CL emission half-width on electron concentration were used for this purpose; the concentration was determined to 15% accuracy. This method cannot be applied in the vicinity of a p–n junction, where material is compensated. As was shown later (Ref. 61), one can construct calibration curves for this technique and also determine acceptor concentrations from them.

It should be noted that reliable identification of layered impurity inhomogeneities caused by aggregation of impuri-

ties at dislocations is possible only in samples with small dislocation densities ($N_{disl} < 10^4$ cm^{-2}).[62] In some cases inhomogeneity in the doping distribution is caused by sample dislocations.[63,64] When a GaAs:Te crystal is bent, a decrease in SEM CL radiation is observed from the strongly deformed regions. After brief heating (700°C, 15 minutes) the intensity of CL begins to grow, almost reaching the CL intensity from nondeformed areas. This phenomenon is connected with the annealing of dislocations and redistribution of doping impurities.[65] In some cases a new peak in the CL spectrum is observed in the vicinity of dislocations; the contrast at dislocations is explained by the presence of point defects (gallium vacancies) and their active interaction with tellurium.[66,67]

A sign change in the contrast at the image of a dislocation with a change of current direction was observed in GaAs:Se in the CL mode.[64] The relative CL intensity has been measured, and from it the concentration of Se has been determined in the vicinity of a dislocation; the intensity was observed to be a minimum at the center of dislocation (Fig. 9a). The relaxation time of the CL signal with pulsed excitation was also a minimum at the same place (Fig. 9b). Detailed investigations have shown that selenium and silicon interact with dislocations to a much lesser extent than tellurium.[68]

In studying GaAs diodes in the CL mode a change in contrast was discovered near the p-n junction whose position was determined from a maximum in the signal current induced by an electron probe (of the induced current). Detailed analysis of p-n junction images has been carried out in Refs. 64,69–71.

The SEM CL method was used for the first time for the determination of values of important semiconductor parameters, i.e., the minority carrier diffusion length, the surface recombination rate and the thickness of the "dead" layer on the semiconductor surface of GaAs samples.[72,73] The primary advantage of the CL method compared to the induced current method is that no electrical contact with the sample is needed; likewise there is no need for a p-n junction or Schottky barrier. Values of the parameters listed above were found by comparing the theoretical and experimental CL intensity dependence on the accelerating voltage. In calculating the theoretical dependence the electron-hole pair generation function was approximated by a Gaussian curve; a possible nonlinear dependence of the CL intensity on the probe current (the nature of which was not quite clear), was taken into account in Ref. 73. The accuracy of this method was not very high simply because CL absorption in the sample was not taken into consideration. A slightly modified method for determining the diffusion length from CL radiation was suggested in Ref. 74. By taking into account the self-absorption of CL radiation on its exit from the sample it was possible to determine the semiconductor parameters more accurately and to explain the shift of the spectral peak towards lower energies.[75] Self-absorption of radiation in the sample, as was shown in Ref. 76, can significantly limit how deep into the sample one can obtain information in the CL mode; this fact must always be taken into account for large values of the absorption coefficient.

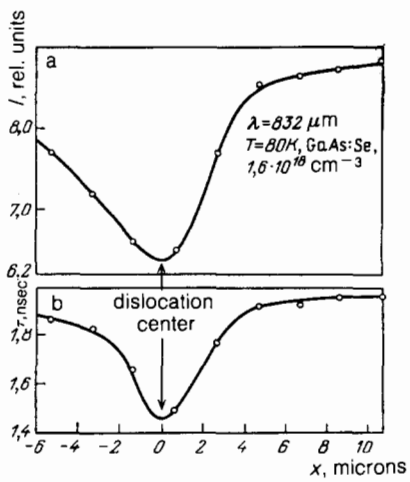

FIG. 9. Variation of CL intensity I (a) and CL relaxation time τ (b) near a dislocation in GaAs: Se as a function of the probe position x relative to dislocation center.

$Ga_{1-x}Al_xAs$. One of the most important problems in the study of these alloys is to determine the dependence of the emission spectrum on chemical composition, and the region of transition from indirect to direct-gap semiconductors, since the direct-gap compounds have the largest efficiency.[77–79] Parameters describing the temporal, spectral and temperature behavior of radiation from $Ga_{1-x}Al_xAs$ LEDs also have been measured. Introducing structural defects in GaAlAs by neutron irradiation leads to selective quenching of the emission band due to recombination via a level related to zinc doping. This could be seen in the falloff in luminescence and the shift of the spectral peak towards higher energies. Annealing of samples did not result in any changes.[80]

GaP. Many papers have been published on research involving GaP epitaxial layers and p-n structures in connection with the wide spread use of this material for preparation of red, green and yellow LEDs. This application stimulated attempts to predict the electroluminescent efficiency of future LED's from results of local SEM CL. For example, during research on red GaP:ZnLED's[69,71,81,82] a correlation was found between the distance from the p–n junction to the region of CL decrease (Fig. 10; for these samples the "dip" of total CL in the area of the p-n junction was absent) and the LED efficiency in the electroluminescent mode[71], and

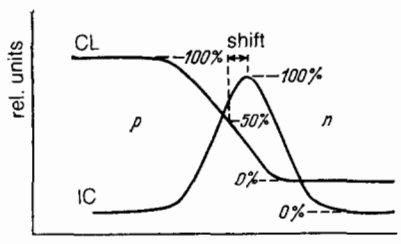

FIG. 10. Distribution (along a scanning line) of the induced current (IC) and integrated cathodoluminescence (CL) intensity for a GaP LED, demonstrating the shift between the IC curve peak (the position of a p-n junction) and the 50 percent point of the CL curve.[71] A large shift corresponds to a low efficiency LED.

the influence of thermal processing of the initial structures was analyzed.[82] Following a method described in Ref. 73 nomograms were constructed in Ref. 83, from which it was shown that in the unfocused beam mode, when saturation of recombination centers is absent, one can measure minority carrier diffusion lengths in GaP:Zn,O.

In order to obtain green LED's, gallium phosphide is doped by adding isoelectronic nitrogen. In an optically active state the nitrogen atoms, which substitute for phosphorus atoms, form traps. These traps bind electrons and holes with the formation of an exciton, whose recombination leads to the appearance in the GaP:N spectra of the A and NN lines (an exciton bound to a single nitrogen atom and to neighboring pairs of nitrogen atoms respectively). These lines are accompanied by phonon satellites of which the strongest is an A–LO phonon. These lines can be well resolved at low temperature (see Fig. 4); and the concentration of nitrogen can be estimated from ratio of NN and A lines.[29] This method, however, can lead to significant errors, due to the fact that emission from the line A undergoes self-absorption when passing through GaP:N. This fact was used in Ref. 84 to determine the local concentration of nitrogen from the degree of self-absorption of line A, by reconstructing its true intensity from the lines A–LO and A–2LO (the relative intensities of all three lines obey the Poisson law).

Emission from the p- and n-regions of p-n structures is substantially different when nitrogen doping is implemented not only in the n-region, but also in the p-region. At low temperatures, a significant contribution in the p-region comes from recombination via donor-acceptor Zn–Te pairs, changing with increasing temperature to hole-donor recombination. If, additionally, nitrogen is present in the p-region, nitrogen lines appear on "pedestals" of bands listed above.[34] The presence of various activators for red and green emission from GaP made it possible to produce yellow and orange GaP LED's by simultaneous excitation of luminescence in the red and green bands of the spectrum. The use of local CL method makes it possible to determine the contributions of radiative recombination mechanisms by cleaving p-n structures with complex doping, such as p-GaP:(Zn, O,N) -n-GaP: (Te,N).[85] It was discovered that the different recombination mechanisms interact with one another. This can be seen in Fig. 11 which shows the distribution of emission intensity for the green (I_1) and red (I_2) bands across a p-n structure cleavage plane as the oxygen concentration is increased. It can be seen that with the increase of the red band intensity the green band intensity decreases. The red band peak in efficient yellow and orange LED's is shifted closer to the p-n junction, and in the most efficient structures a red band was observed also in the n-region, which was accompanied by a drop in intensity of the green band in the n-region.

The presence of a large number of radiative recombination channels competing with each other and also with nonradiative recombination channels, is the cause of the complex variation of CL spectra (especially for structures with yellow emission) caused by neutron irradiation.[86] This could be interpreted as "selective" band quenching; in fact,

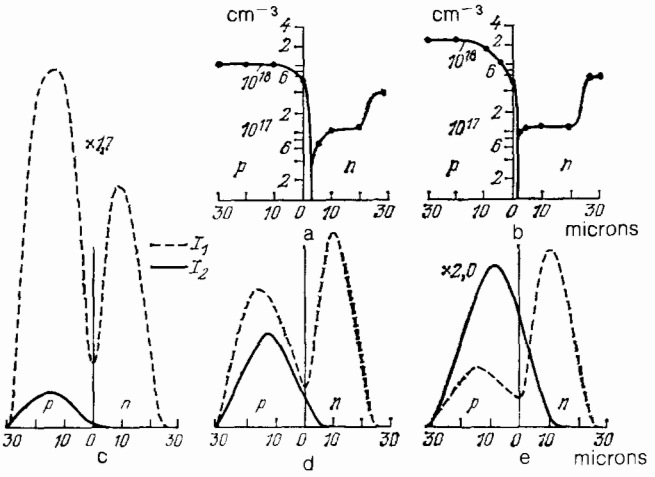

FIG. 11. Typical carrier concentration as a function of distance from a junction measured across the cleaved surface of efficient yellow (a) and orange (b) LED GaP—structures, and the intensity distribution of monochromatic CL in the green (I_1) and red (I_2) bands across cleaved surface for a gradual increase in oxygen concentration in the p-region for $T = 300$ K, $U = 30$ kV, $I_3 = 2 \cdot 10^{-7}$ A (c–e).[85]

however, this is a demonstration of the variation of the effective level of excitation due to the injection of a large number of nonradiative centers.

A number of papers is devoted to investigation of CL with dislocations in GaP[87,88] or of areas in the immediate vicinity of dislocations. Comparison of CL microphotographs with thinned-sample photographs taken with an electron microscope in the transmission mode gives direct proof that the dark points on CL images correspond to crystal surface dislocations. Various types of dislocations—screw type, edge type, etc., result in dark spots on the CL images of the same size and intensity.[89] The size of dark spots on CL images depends, generally speaking, on various factors—the size of the pair-generation area, the minority carrier diffusion length, the electron probe diameter, etc. The minimum size of dislocation images in GaP in the CL mode was about 1 μm[90] at 15 kV and was in practice limited by the size of a diffusion length. In most works on the study of defects in the CL mode, images in the induced current mode were also given for comparison purposes, and not only structural defects but also doping non-uniformities were observed.[91] It is possible to observe dislocations and estimate their density in this mode up to dislocation densities of $\sim 10^{-7}$ cm^{-2}, which in turn makes possible the study of dislocations formed during the growth of layers, as well as dislocations created during deformation.[92]

The high spatial resolution of CL methods and of induced SEM currents has made it possible to undertake the study of individual dislocations.[93–95] The CL spectra and minority carrier lifetimes τ in GaP have been measured at dislocations and away from dislocations; it was found that the CL spectra differed insignificantly, while the time τ at dislocations decreased by 30–50%.[96] Dislocations behaved as efficient centers of nonradiative recombination, as a result of which they are responsible for a significant part of total CL radiation; this becomes even more evident with an in-

crease in dopant concentration. This fact served as direct confirmation of the role of impurity segregation at dislocations. The efficiency of dislocations as centers of nonradiative recombination in weakly doped samples or samples where dislocations are created by deformation is significantly smaller; furthermore, it is determined not by segregation of impurities, but by the dislocation structure. Generally speaking, variations in lifetime τ and impurity segregation taking place near a dislocation are smooth; however, the determination of these quantities requires specific models and computer calculations.[97]

In GaP doped by Te or S, for carrier concentration of approximately $(2–7)\cdot 10^{17}$ cm^{-3} it is possible to observe the creation of defects that are unrelated to dislocations (apparently inclusions of the second phase) that act as efficient centers of nonradiative recombination. They appear at a sufficiently high concentration of Te or S and are accompanied by the formation on the crystal surface of small pits, whose density grows with increasing Te or S concentration. Areas with accumulations of these small pits had sharply reduced radiative recombination. Undoped GaP crystals did not have these pits, which shows that these defects are related to the presence of the doping impurity and its behavior during the growth process.[98] The study of recombination efficiency at structural defects, in particular of dislocations, is important from the point of view of studying degradation processes in optoelectronic devices[99–101] and determining optimal methods of thermal processing in order to increase the efficiency of light emitting structures made from GaP:N.[102–104]

The distribution of the total CL intensity across a p-n structure depends strongly on the manufacturing process and on the excitation level. For low levels of excitation, radiation from the p-region exceeds radiation from the n-region[105,106]; for a long time this was explained by invoking the higher efficiency of the p-region and the need to supply preferential injection of carriers into the p-region. For high levels of excitation the situation changes to its opposite[106] (Fig. 12). In general, for the green GaP p-n structures, in the p-n junction area there is always visible a dip in the total CL intensity caused by "spreading" of carriers by the p-n junction field; this spreading can be reduced by applying a positive bias.[107] In this case one more minimum of total CL intensity in the n-region near p-n junction is observed that cannot be suppressed by forward bias of the p-n junction. This minimum was due to the efficiency of nonradiative recombination in the vicinity of the p-n junction as a result of which the efficiency of the studied LED's in the luminescent mode was low.

More detailed analyses of the temperature dependences of local CL spectra from GaP p- and n-regions of p-n structures, the intensity dependences of individual spectral lines on the level of excitation, and local CL analysis of areas with different concentration of nonradiative recombination centers on surfaces of the layers[108] have revealed details which were previously ignored. It turns out that under illumination with the narrow nitrogen lines the spectrum always contains broad bands, whose intensity grows with increasing nitrogen concentration. The intensities of these lines are comparable to the intensities of the nitrogen lines, and they appear mostly in spectra from the p-region; for low levels of excitation their intensity may significantly exceed the intensity of the nitrogen lines (Fig. 13). It is an interesting fact that these lines are present only in spectra from the nitrogen-doped areas, and are absent in the spectra of areas without nitrogen; and that their structure reproduces the nitrogen line structure. All this indicates a relationship between the recombination responsible for these lines and injected nitrogen. More detailed analysis of the dependence of this recombination on thermal processing for different initial nitrogen concentration has made it possible to propose a model for the recombination center—a nitrogen atom on a gallium site bound to an optically active nitrogen on a phosphorus site.[108] Without this bond a nitrogen atom replacing gallium behaves as an efficient nonradiative center. Such behavior is also suggested by the kinetics of the total CL in n-GaP:N with variation of the excitation level and temperature (Fig. 14).[109]

At 300 K and at high levels of excitation it is not unu-

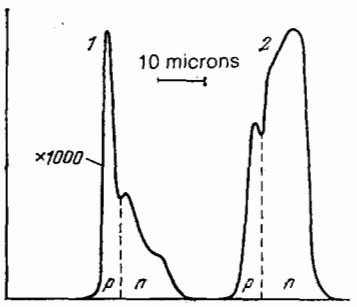

FIG. 12. Distribution of integrated CL intensity across a GaP p-n structure for low (1) and high (2) levels of excitation.[106]

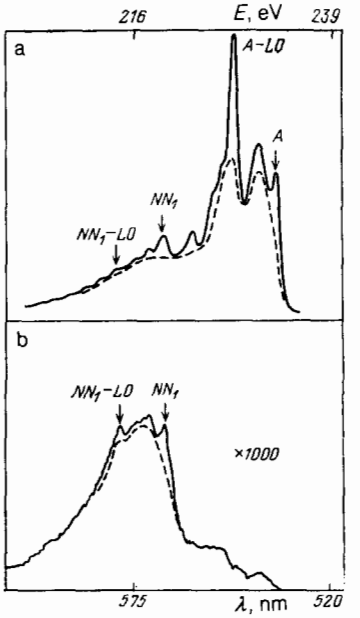

FIG. 13. CL spectra from p-GaP structures at 114 K for high (a) and low (b) levels of excitation. The background signal from the broad bands is shown by a dashed line.[106]

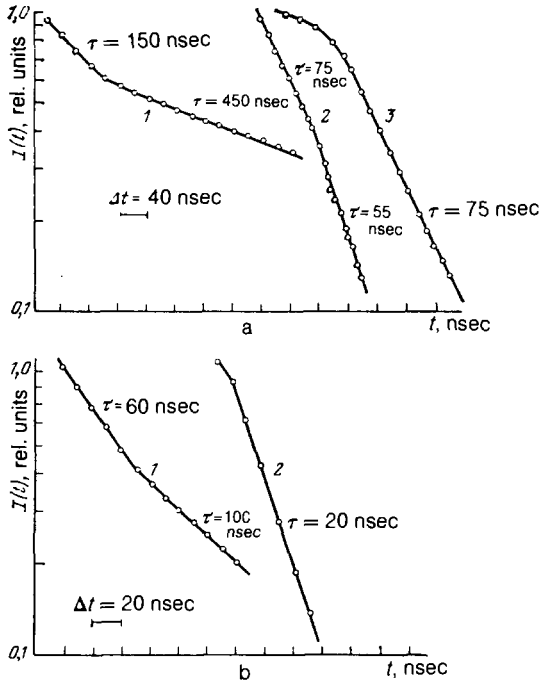

FIG. 14. Decay of integrated CL intensity $I(t)$ (on a logarithmic scale, relative units) for the liquid phase of n-GaP samples of various growth runs for different temperatures and probe currents.[109]

sual to have sharp breaks in the curves describing the decay of the relative intensity of CL $I(t)$ on a logarithmic scale when τ changes from larger to smaller values. Increasing the level of excitation leads to the large-τ portion of the curve becoming the dominant portion, while the small-τ portion disappears (see Fig. 14a). On the other hand, for low levels of excitation an exponential decay is observed, with τ corresponding to τ_{min} on the broken curves. This feature of the kinetics can be explained by nonradiative recombination on multiply-charged centers, whose charge state during the relaxation process is changed because of the variation in free carrier concentration. At 110 K a number of samples reveal for low levels of excitation the influence of "capture" centers which give rise to the appearance of long "tails" in the decay curves and bends at the transitions from smaller to larger τ (see Fig. 14 b).

It must be noted that in one of the first publications on the SEM study of CL local kinetics[110] these bends in the CL relaxation were observed, but no explanation was given.

$GaAs_{1-x}P_x$. The first works on SEM study of $GaAs_{1-x}P_x$ alloys were related to a study of the behavior of the CL intensity and absorption edge as a function of composition, which was monitored by using x-ray microanalysis data.[111] The dependence of CL spectra on the excitation level for compounds close to GaP ($x = 0.96$) is analogous to the dependence observed in GaP[106,112]: wide bands form "pedestals" under the nitrogen lines and dominate the spectrum at low levels of excitation, and radiation from the p-region is significantly larger than radiation from the n-region. For smaller x ($x = 0.86$) when the nitrogen lines are not resolved at 114 K, the long-wave length part of the spectrum increases with a decrease in excitation level.[112] The temperature dependence of the integrated CL for indirect $GaAs_{1-x}P_x$ compounds lightly doped with nitrogen was studied in Ref. 113, where it was confirmed that for the temperature range $350 \geqslant T \geqslant 150$ K, the temperature dependence is determined by thermal ejection of electrons and holes and by the decay of excitons bound on isolated nitrogen atoms.

A depth profile study of the inhomogeneous distribution of radiative characteristics in $GaAs_{1-x}P_x$ epitaxial layers has demonstrated the strong influence of variation in the temperature and growth conditions on the efficiency of local CL across the thickness of a layer.[114] The way the structures were cooled after growth also had a strong influence, since residual elastic stress causes structural defects to form that are centers of nonradiative recombination. The significant role played by dislocations in the (100) plane perpendicular to the growth axis of a layer was an additional discovery; these dislocations cause significantly more reduction of the CL than tilted dislocations in p- and n-layers of $GaAs_{0,6}P_{0,4}$.[115]

$Ga_{1-x}In_{1-x}P$. CL SEM studies in $Ga_xIn_{1-y}P$ crystals were carried out in Refs. 116, 117 with the purpose of finding growth defects and areas with varying intensity of radiation. The small shift in the luminescence peak was explained by residual stress.

$Ga_{1-x}Al_xP$. $Ga_{1-x}Al_xP$ solid solutions have a slightly larger forbidden gap than GaP. The CL intensity of a n-$Ga_{1-x}Al_xP$:Te layer decreases with increasing aluminum content, because of the increasing density of dislocations which provide a channel for nonradiative recombination. At 300 K the spectrum is dominated by absorption edge radiation in the green area of the spectrum, corresponding to recombination of free excitons accompanied by the emission and absorption of longitudinal phonons. At 110 K for $x \geqslant 0.1$, the spectrum is dominated by a 1.94 eV band in the red region of the spectrum, whose maximum is almost independent of composition, temperature and level of excitation. The intensity of this band increases in the direction of the heterojuncture (see Fig. 3), and also grows with increasing aluminum content (Fig. 15). The nature of this band is probably related to a defect; specifically, a dislocation "mismatch", caused by the lattice mismatch between the GaP substrate and the solid solution.[25] The same band is observed in local spectra from the p-region at 110 K and in a number of samples its intensity is larger than the intensity from the n-region. The variations in local CL spectra from the GaAlP p-region with temperature and aluminum content are given in Ref. 118. The fact that the red band is related to the presence of dislocation "mismatch" was confirmed by results of the CL analysis of p-GaAlP layers of different thicknesses, in which the transition from elastic to plastic deformation of the p-layer (i.e., formation of a dislocation network) for samples with given composition was accompanied by a sharp increase in the relative intensity of this band.

Because it is technologically difficult to introduce isoelectronic nitrogen doping into $Ga_{1-x}Al_xP$ during the process of liquid epitaxy, an attempt was made in Ref. 119 to introduce nitrogen by ion implantation. After processing at 950°C, bands related to the presence of optically active nitrogen appear in the spectrum. But the long-wavelength bands

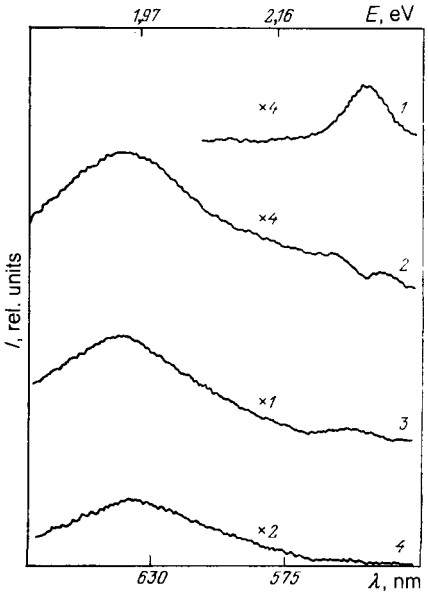

FIG. 15. CL n-$Ga_{1-x}Al_xP$ spectra at 114 K for different compositions.[25] $x = 0$ (1), 0,1 (2), 0,3 (3) and 0,5 (4).

that, as was mentioned earlier, are determined by the presence of structural defects dominate the spectrum.

GaN. Direct-band gap GaN has a wide energy gap (3.5 eV), and its emission can in principle cover the entire visible region. CL radiation from GaN m-i-n structures was observed in Ref. 120 in the blue region of the spectrum. The GaN layer consisted of many identically oriented crystallites. Accumulation of zinc was observed at the crystallite boundaries and at the interface surface between the metal and the high resistivity layer. As a result of local heating caused by the electron beam, zinc diffusion takes place, with zinc atoms displacing gallium atoms to become centers of efficient nonradiative recombination. This can explain the anomalously long time scale for CL kinetics, in which a maximum in the CL is clearly visible in the time variation[121] (Fig. 16). Depending on the growth conditions and zinc concentration, the crystal structure and emission spectrum of GaN can be varied substantially. Zinc forms centers of blue, green and yellow luminescence bands, coupled with various structural defects, and the position of the emission peak depends on the intensity ratio of these bands.[122] A significant increase in emission intensity was observed for electron-beam-irradiated GaN:Zn. The relaxation processes

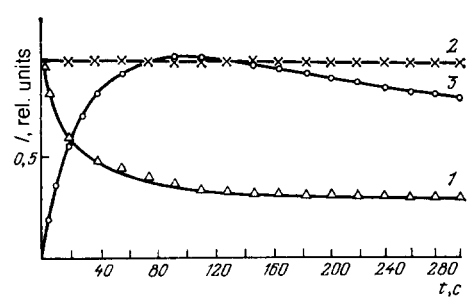

FIG. 16. CL kinetics of CdS (1), ZnO (2) and GaN: Zn (3) in the first 5 minutes after switching on a stationary electron probe with a current density of 100 A/cm² ($U = 20$ kV).[121]

after irradiation depend strongly on temperature and have two clearly defined components—one short-lived and one long-lived.[123] The existence of the latter component has made it possible to use the luminescence for recording information.[124] When grown on sapphire GaN had a "skeleton" growth mechanism, in which pyramids are visible on the surface of the epitaxial layer.[125,126] The CL radiation consisted of a single band and was distributed in a very nonuniform way across the surface due to quenching of the CL caused by uncontrolled impurities.

5.2. II-VI Compounds, ternary compounds based on them and dielectrics

Powder-like phosphors and ionic crystals having efficient luminescence in the visible spectrum were some of the first objects of research using the SEM CL mode. The temperature dependence of the CL intensity was obtained for the ionic crystals NaCl and KCl, and the effect of ion etching on local CL properties of these crystals was discovered.[127–129] The main trend in phosphor studies was towards finding the dependence of spectra and luminescence efficiency as a function of the phosphors' lattice crystal structure, and of accelerating voltage and beam current. Examples of such studies are works on ZnS-CdS phosphors.[130–131]

Investigations of CL spectra from various structural phases were carried out for samples of ZnS, ZnTe, ZnSe and ZnO.[30,132–141] Due to spectral differences between the various phases, it was possible using the monochromatic CL mode to make the different phases visible, as is easily seen for ZnSe in Fig. 5.[30]

A great deal of research was carried out in CdS concerning the effects of electronic and ionic irradiation of single crystals on the CL spectra.[142–145] Because of the radiation-induced effects redistribution of spectral line intensities was observed in CL spectra which made it possible to study migration and interaction of defects. In Ref. 146 a study was made of the effects of plastic deformation on the CL spectra in CdS, and in Refs. 147,148 an attempt was made to establish the relationship between the defects formed during the surface processing of single crystal CdS, and uniformity of emission, estimated from the intensity of the blue band (free-exciton annihilation).

Cathodoluminescence SEM studies have elucidated a number of details in more complex structures. Investigation of the spectra of p- and n-type $ZnSe_xTe_{1-x}$ diode structures has shown that the main contribution to electroluminescence in these structures comes from recombination in the p-regions close to the p-n junction.[134] For ZnSe–CdTe structures with a heterojunction a source of electroluminescence instability was identified, which was related to defects in the ZnSe layer.[149] In Cu_2S–CdS photoelements, a copper doped CdS layer was found in the vicinity of the interface.[150]

5.3. Narrow-gap semiconductors

Some of the first works on the SEM study of infrared CL involved $GaAs_xSb_{1-x}$ compounds.[151,152] In these works PbS photoresistors were used to record the radiation. The use of synchronous detection makes it possible to record

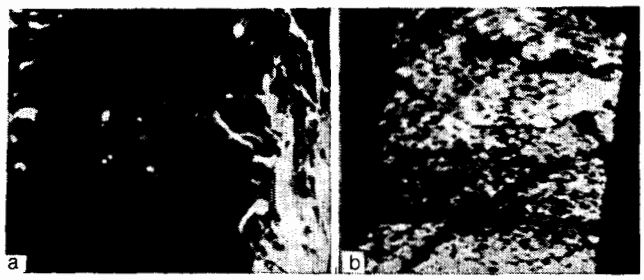

FIG. 17. Microphotograph of the surface near a GaSb tunnel diode at 300 K viewed by secondary emission (a) and integrated CL (b) modes.[151]

radiation up to 2.5–3 μm. Using such a detector, tunnel and luminescent diodes based on gallium antimonide were analyzed at 100 and 300 K. Figure 17 shows microphotographs of a cleaved sample of such a diode at 300 K taken with secondary electron emission (a) and CL(b). The radiation comes mainly from the n-region. The p-region contains a large number of inhomogeneities, caused by the zinc doping, as a result of which the probability of nonradiative recombination increases and that of CL decreases.

In other works a germanium photodiode was used as a detector (having a wavelength recording range of 1–1.8 μm.[153] The images of the epitaxial heterojunction structures obtained in the CL mode reveal the existence of periodic CL intensity variations in the form of a dark line pattern in the layers in the vicinity of the heterojunction. The distance between the lines with reduced CL intensity in layers with variable composition depended on the gradient across the epitaxial layer and varied from μm to 50 μm for a change of composition gradient from 0.5 to 0.05 mol% of gallium antimonide per micron.

LED and laser epitaxial InGaAsP double-heterostructures were studied in Refs. 53,154,155 using the integrated CL mode ($\lambda = 1.0$–$1.6\,\mu$m). Characteristic defects responsible for nonradiative recombination were seen on CL images of the active layer of the structure. Together with dislocations penetrating from the substrate into the growing active and emitter layers, and "inclusions" of various phases of 2–6 μm size, the samples had layered inhomogeneities, which give rise to corresponding light and dark stripes on the CL images (Fig. 18).[155] These complex inhomogeneities were characterized by increased intensity of radiation from the active layer of the heterostructure; the cause of this is apparently the escape of the radiation to the surface, which occurs due to poor epitaxial growth of the top layer. Together with the "inclusions" of phases of unknown composition and having luminescence of low intensity, individual crystallized aggregates of InP were found in the active layer of the alloy that might originate from partial dissolving of the substrate in the liquid epitaxial layer. LED's made from structures with a high density of nonradiative defects that propagated through both layers during the growth process in most cases did not have rectifying properties. This was due to "shorting out" of the heterojunction by these inhomogeneities, which behaved like current conducting microchannels.

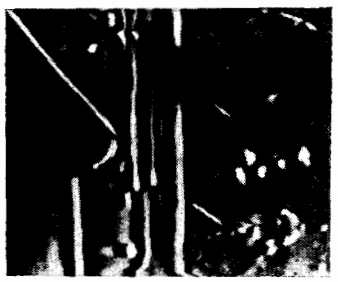

FIG. 18. Monochromatic CL image corresponding to emission from the active layer ($\lambda = 1.5\,\mu$m) of the surface of a InGaAsP–InP double heterostructure viewed from the side of an emitter layer.[155]

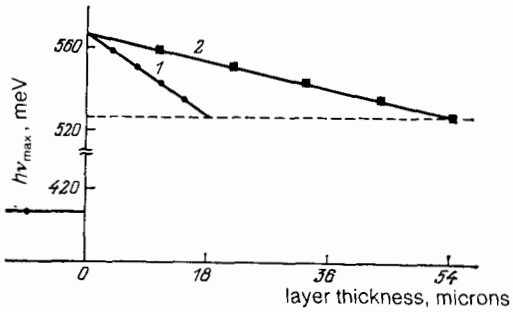

FIG. 19. Coordinate dependence of energy peaks of local CL spectra (the width of the energy gap) across the cleaved surface of an epitaxial InAsSbP–InAs heterostructure with 18 μm (1) and 55 μm (2) thick variable-gap layers.

Epitaxial heterostructures InGaAs, InAsP and InAsSbP with variable energy gaps prepared by the method of liquid epitaxy were studied in Refs. 53,154. CL spectra obtained using a parallel shift of the electron probe across the cleaved surface of a sample, made possible the measurement of local values of the energy gap E_g in heterostructures and the determination of layer thicknesses and heterojunction boundaries. The position of the peak in CL spectra, obtained from different areas of an epitaxial InGaAs layer, remained unchanged up to thicknesses of about 100 μm, which demonstrated the constancy of composition in the direction of the growth of a layer. For epitaxial layers of InAsP and InSbP solid solutions a linear change in peak energies of local CL spectra was the rule, with the energy gap decreasing toward the surface of the sample (Fig. 19). The measured value of the gradient of E_g was 1.5 meV/micron.

The first study of local CL in PbS was done in Ref. 156. Further studies of PbS activated by film oxidation in the modes of induced β-conductivity in SEM CL have made it possible to observe in them substantial inhomogeneities in their photoelectrical and luminescent properties.[152,157] The active areas of photosensitivity and luminescence had a size of about $3 \cdot 10\,\mu m^2$, which exceeded significantly the size of crystallite grains (Fig. 20). The characteristic grain texture

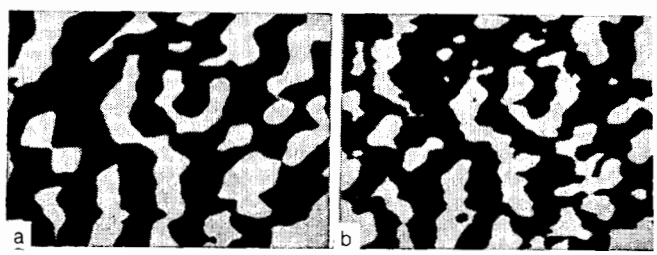

FIG. 20. Image of the same area of a polycrystalline PbS film in the induced β-conductivity (a) and integrated CL (b) modes.[157]

of the surface determined the orientation of larger photosensitive areas. Using studies of the oxygen distribution on film surfaces by Auger spectroscopy, the inhomogeneity of oxygen absorption from some areas of films during thermal processing was established. Areas with increased oxygen content coincided with areas having high photosensitivity and luminescence.

[1]J. I. Goldstein, Scanning Electron Microscopy and X-ray Microanalysis, Plenum Press, N. Y., 1981 [Russ. transl., Mir, M., 1984, V. 1, p. 303; V. 2, p. 348].
[2]N. V. Koronovskiĭ, G. V. Saparin, V. I. Sluev, and G. V. Spivak, Dokl. Akad. Nauk SSSR. **225**, 667 (1975).
[3]G. V. Spivak, M. K. Antoshin, G. V. Saparin, G. V. Dobrovolskiĭ, and S. A. Shoba, Vestn. Mosk. Univ. Biol. Pochvoved; No. 3, 81 (1973).
[4]G. V. Spivak, G. V. Saparin, M. K. Antoshin, R. A. Bochko, and V. A. Lodygin, Vestn. Mosk. Univ. Geol., No. 6, 44 (1973).
[5]G. V. Spivak, R. A. Bochko, G. V. Saparin, and M. K. Antoshin, *ibid.* p. 48.
[6]M. K. Antoshin, N. P. Il'in, G. V. Spivak, and G. V. Saparin, In: "Lunnyĭ grunt iz morya isobiliya" (Lunar soils from the Sea of Abundance), Nauka, M., 1974, p. 529.
[7]G. Remond, J. Lumin. **15**, 121 (1977).
[8]R. F. W. Pease and T. L. Hayes, Nature **210**, 1049 (1966).
[9]W. Bröcker and G. Pfefferkorn, In: SEM (Scanning Electron Microscopy), 1979 AMF O'Hare, Il.: SEM Inc. 1979, V. 2, p. 125.
[10]M. Hollenberg, J. Erickson, and M. Allan, J. Histochem. Cytochem. **21**, 109 (1973).
[11]G. V. Saparin, V. I. Sluev, and G. V. Spivak, Izv. Akad. Nauk SSSR, Ser. Fiz. **40**, 2402 (1976) [Bull. Acad. Sci. USSR, Phys. Ser. **40** (11), 100 (1976)].
[12]E. M. Hörl and E. Mügschl, In: Electron. Microscopy, Proc. of 5th European Congress of Electron Microscopy, Manchester, 1972, p. 502.
[13]R. Holm, In: SEM/1975, Chicago, Il.: IITRI, 1975, p. 433.
[14]R. Fuchert and H. Selzer, In: Microscopie electronique, Proc. of 7th Inter. Congress of Electron Microscopy, Grenoble, 1970, Vol. 1, p. 631.
[15]G. Pfefferkorn, In: Ref. 13, p. 631.
[16]a) G. Pfefferkorn, W. Brocker, and M. Hastenrath, In: SEM. 1980/1 AMF O'Hare, Il.: SEM, Inc., 1980, V. 1, p. 251; b) D. B. Holt and S. Datta, *ibid.*, p. 259; c) M. Hastenrath and E. Kubalek, In: SEM 1982/1. AMF O'Hare, Il.: SEM, Inc., 1982, V. 1, p. 157; d) G. V. Spivak, G. V. Saparin, and M. K. Antoshin, Usp. Fiz. Nauk **113**, 695 (1974) [Sov. Phys. Usp. **17**, 593 (1975)].
[17]W. Brocker and G. Pfefferkorn, In: SEM 1978/1. AMF O'Hare, Il.: SEM, Inc., 1978, V. 1, p. 333; in Ref. 16a), p. 298; In: "Practical scanning electron microscopy," Eds. G. Goldstein, H. Jackovits, [Russ. transl., Mir, M., 1978, p. 624].
[18]M. S. Epifanov, E. A. Bobrova, and G. N. Galkin, Fiz. Tekh. Poluprovodn. **9**, 1529 (1975) [Sov. Phys. Semicond. **9**, 1008 (1975)]; V. S. Vavilov, G. N. Galkin, and M. S. Epifanov, Litov. Fiz. Sb., **21** (4), 57 (1981).
[19]G. V. Spivak, L. F. Komolova, V. I. Sluev, G. V. Saparin, and M. K. Antoshin, Pis'ma Zh. Eksp. Teor. Fiz. **21**, 38 (1975) [JETP Lett. **21**, 17 (1975)].
[20]D. A. Cusano, Solid State Commun. **2**, 353 (1964).
[21]G. V. Spivak, G. V. Saparin, V. I. Sluev, S. S. Elovikov, and M. V. Bykov, Mikroélektronika **6**, 64 (1977) [Sov. Microelect. **6**, 47 (1977)].
[22]V. E. Umanskiĭ, S. G. Konnikov, D. Z. Garbuzov, É. V. Tulashvili, I. N. Arsent'ev, and I. V. Doĭnekina, Fiz. Tekh. Poluprovodn. **16**, 1496 (1982) [Sov. Phys. Semicond. **16**, 1955 (1982)].
[23]a) J. Llopis, J. Piqueras, and L. Bru, J. Mater. Sci. **13**, 1361 (1978); b) C. Ballesteros, J. Llopis, and J. Piqueras, In: Electron Microscopy, 1982, Proc. of 10th Intern. Congress of Electron Microscopy, Hamburg, 1982, V. 1, p. 273.
[24]M. Sh. Akchurin and V. G. Galstyan, Dokl. Akad. Nauk SSSR **252**, 870 (1980) [Sov. Phys. Dokl. **25**, 411 (1980)] Izv. Akad. Nauk SSSR Ser. Fiz. **44**, 2134 (1980) [Bull. Acad. Sci. USSR, Phys. Ser. **44** (10), 119 (1980)]; M. Sh. Akchurin, V. G. Galstyan, V. R. Regel' and V. N. Rozhanskiĭ, Poverkhnost' (The Surface) No. 3, 119 (1983).
[25]V. N. Bessolov, E. S. Dobrynina, V. I. Petrov, and Yu. P. Yakovlev, Fiz. Tekh. Poluprovodn. **15**, 694 (1981) [Sov. Phys. Semicond. **15**, 395 (1981)].
[26]Zh. I. Alferov, In: "Fizika segodnya i zavtra" (Physics today and tomorrow), Ed. V. M. Tuchkevich, Nauka, Leningrad, 1973, p. 61. B. L. Sharma and R. K. Purokhit, In: "Poluprovodnikovye geteroperekhody" (Semiconductor heterojunctions), Soviet Radio, M., 1979; A. G. Milnes and D. L. Feucht, Heterojunctions and metal-semiconductor junctions, Academic Press, N. Y. 1972 [Russ. transl., Mir, M., 1975].
[27]G. A. C. Jones, B. R. Nag, and A. Gopinath. a) In: SEM 1973, Chicago, Il.: IITRI, 1973, p. 309; b) J. Phys. Ser. D **7**, 183 (1974).
[28]G. Oelgart, R. Stegmann, and L. John, Phys. Status Solidi **A59**, 27 (1980).
[29]D. R. Wright, J. C. H. Birbeck, J. W. A. Trussler, and M. L. Young, J. Phys. **D6**, 1622 (1973).
[30]P. M. Williams and A. D. Yoffe, Nature **221**, 952 (1969).
[31]G. P. Barsanov, G. V. Spivak, G. V. Saparin, M. K. Antoshin, and I. V. Nesterov, Vestn. Mosk. Univ. Geol. No. 6, 40 (1973).
[32]M. A. Velednitskaja, V. N. Rozhanskij, G. V. Saparin, L. F. Komolova, J. Schreiber, and O. Brummer, Phys. Status Solidi **A32**, 123 (1975).
[33]E. I. Rau, A. Yu. Sasov, and G. V. Spivak, Scanning **3**, 242 (1980); G. V. Spivak, E. I. Rau, and A. Yu. Sasov, Usp. Fiz. Nauk **139**, 165 (1983) [Sov. Phys. Usp. **26**, 84 (1983)].
[34]Yu. A. Golubev, V. I. Petrov, G. V. Spivak, and A. É. Yunovich, Izv. Akad. Nauk SSSR. Ser. Fiz. **40**, 2334 (1976) [Bull. Acad. Sci. USSR, Phys. Ser. **40** (11), 38 (1976)].
[35]V. I. Sluev, G. V. Saparin, and G. V. Spivak, Vestn. Mosk. Univ. Fiz. Astronomiya **17**, 486 (1976).
[36]M. S. Antoshin, G. V. Spivak, and A. E. Yunovich, In: Ref. 14, V. 1, p. 251.
[37]J. Lebiedzik, E. W. White, and R. I. Bhalla, Rev. Sci. Instrum. **45**, 451 (1974).
[38]M. K. Antoshin, G. V. Spivak, A. E. Luk'anov, E. I. Rau, O. A. Ushakov, A. I. Akishin, G. A. Tokarev, V. E. Lyamov, and I. Bartel', Izv. Akad. Nauk SSSR **36**, 1954 (1972) [Bull. Acad. Sci. USSR, Phys. Ser. **36**, 1727 (1972)].
[39]M. Boulou and D. Bois, J. Appl. Phys. **48**, 4713 (1977).
[40]A. Steckenborn, J. Microsc. (Oxford) **118**, 297 (1980).
[41]S. K. Obyden, S. I. Popov, and G. V. Saparin, Poverkhnost' (The Surface) No. 11, 97 (1982).
[42]O. V. Kononov, V. I. Sluev, G. V. Saparin, and G. V. Spivak, Geol. Rudn. Mesto rozhd. (Geology of ore deposits) No. 1, 111 (1976).
[43]S. K. Obyden, G. V. Saparin, G. V. Spivak, A. G. Teplyakov, and S. I. Popov, Izv. Akad. Nauk SSSR Ser. Fiz. **44**, 1142 (1980) [Bull. Acad. Sci. USSR Phys. Ser. **44** (6), 14 (1980)].
[44]S. K. Obyden, G. V. Saparin, and G. V. Spivak, Scanning **3**, 181 (1980).
[45]V. I. Sluev, G. V. Saparin, and G. V. Spivak, Radiotekh. Elektron. **21**, 312 (1976) [Radio Eng. Electron. (USSR) **21**, 75 (1976)].
[46]G. V. Saparin and G. V. Spivak, In: Ref. 9, p. 267.
[47]M. K. Antoshin, L. V. Epifanova, G. V. Spivak, M. V. Chukichev, and E. Braga, Izv. Akad. Nauk SSSR Ser. Fiz. **41**, 939 (1977) [Bull. Acad. Sci. USSR Phys. Ser. **41** (5), 86 (1977)].
[48]R. I. Bhalla and E. W. White. J. Appl. Phys. **41**, 2267 (1970); J. Electrochem. Soc. **119**, 740 (1972); R. I. Bhalla, J. Appl. Phys. **45**, 3703 (1974).
[49]G. V. Spivak, M. N. Filippov, and M. K. Antoshin, Izv. Akad. Nauk SSSR Ser. Fiz. **41**, 876 (1977) [Bull. Acad. Sci. USSR Phys. Ser. **41** (5), 29 (1977)].
[50]I. Kiplawi and A. R. Lang, Philos. Mag. **30**, 219 (1974).
[51]F. A. Gimel'farb, A. V. Govorkov, B. I. Kuzovkin, and V. I. Fistul', Zavod. Lab. (Industrial Laboratory) **7**, 881 (1972).
[52]A. K. Chin, In: Ref. 16c, V. 3, p. 1069.
[53]V. I. Petrov and V. A. Prokhorov, In: Electron Microscopy, 1984; Proc. 8th European Congress of Electron Microscopy, Budapest, 1984, V. 2, p. 417.
[54]M. Cocito, F. Gorgellino, and A. Troia, In: Ref. 23b, V. 2, p. 417.
[55]E. F. Bond, D. Beresford, and G. H. Haggis, J. Microsc. (Oxford) **100**, pt. 3, 271 (1974).
[56]K. Lohnert, M. Hastenrath, and E. Kubalek, In: Ref. 9, V. 1, p. 229.
[57]M. Hastenrath, L. J. Balk, K. Lohnert, and E. Kubalek, J. Microsc. (Oxford) **118**, pt. 3, 303 (1979).
[58]S. M. Davidson, T. J. Cumberbatch, E. Huang, and S. Myhajlenko, In: Institute of Physics Conference Ser. No. 61, The Institute of Physics, London; Bristol, 1982, p. 191.
[59]D. B. Wittry and D. F. Kyser, J. Appl. Phys. **35**, 2439 (1964).
[60]H. C. Casey and R. H. Kaiser, J. Electrochem. Soc. **114**, 149 (1967).
[61]R. S. Gvozdover, V. A. Matveev, V. I. Petrov, and M. A. Stepovich, Izv. Akad. Nauk SSSR Ser. Fiz. **44**, 2145 (1980) [Bull. Acad. Sci. USSR Phys. Ser. **44** (10), 128 (1980)].
[62]F. A. Gimel'farb, A. V. Govorkov, M. G. Mil'vidskiĭ, and V. I. Fistul', Izv. Akad. Nauk SSSR Neorg. Mater. (Inorganic materials) **11**, 1516 (1975).

[63]M. K. Antoshin, E. M. Krasavina, I. V. Kryukova, V. I. Sluev, and G. V. Spivak, Kvantovaya Elektron. (Moscow) **2**, 1969 (1975) [Sov. J. Quantum Electron. **5**, 1069 (1975)].
[64]L. J. Balk, E. Kubalek, and E. Menzel, In: SEM/1976, Chicago, Il., IITRI, 257 (1976).
[65]A. L. Esquivel, S. Sen, and W. N. Lin, J. Appl. Phys. **47**, 2588 (1976).
[66]A. V. Govorkov and L. I. Kolesnik, Fiz. Tekh. Poluprovd. **12**, 448 (1978) [Sov. Phys. Semicond. **12**, 259 (1978)].
[67]A. S. Bruk, A. V. Govorkov, L. I. Kolesnik, and A. M. Loshinskiĭ, Fiz. Tekh. Poluprovod. **16**, 1510 (1982) [Sov. Phys. Semicond. **16**, 966 (1982)].
[68]D. A. Shaw and P. R. Thornton, J. Mater. Sci. **3**, 507 (1968).
[69]B. D. Chase and D. B. Holt, Phys. Status Solidi **A19**, 467 (1973).
[70]V. D. Okunev, B. G. Zakharov, and V. I. Gaman, Radiotekh. Elektron. **18**, 2133 (1973) [Radio Eng. Electron. (USSR) **18**, 1571, 1973].
[71]D. B. Holt, B. D. Chase, and M. Censlive, Phys. Status Solidi **A20**, 459 (1973).
[72]D. B. Wittry and D. F. Kyser, J. Appl. Phys. **38**, 375 (1967).
[73]T. S. Rao-Sahib and D. B. Wittry, *ibid.* **40**, 3745 (1969).
[74]A. B. Ormont, Prib. Tekh. Eksp. No. **2**, 199 (1976) [Instrum. Exp. Tech. **19**, 548 (1976)].
[75]R. S. Gvosdover, V. I. Petrov, E. Ya. Podtyazhkin, M. A. Stepovich, and M. N. Filippov, Izv. Akad. Nauk SSSR Ser. Fiz. **48**, 2378 (1984) [Bull. Acad. Sci. USSR Phys. Ser. **48**, 83 (1984)].
[76]W. Hergert, L. Pasemann, Phys. Status Solidi **A85**, 641 (1984).
[77]F. A. Gimel'farb, A. V. Govorkov, and V. I. Fistul, Izv. Akad. Nauk SSSR Ser. Fiz. **38**, 1409 (1974) [Bull. Acad. Sci. USSR Phys. Ser. **38** (7), 43 (1974)].
[78]F. A. Gimel'farb, A. V. Govorkov, S. G. Grishina, M. G. Mil'vidskiĭ, V. I. Fistul', and S. S. Shefrin, Kristallografiya. **19**, 1115 (1974) [Sov. Phys. Crystallogr. **19**, 692 (1974)].
[79]L. J. Balk, E. Kubalek, and E. Menzel, In: Ref. 13, p. **447**.
[80]V. A. Brzhezinskiĭ, E. S. Dobrynina, V. I. Petrov, and M. V. Chukichev, Izv. Akad. Nauk SSSR, Ser. Fiz. **41**, 991 (1977) [Bull. Acad. Sci. USSR Phys. Ser. **41** (5), 131 (1977)].
[81]W. H. Hackett, R. H. Saul, R. W. Dixon, and G. W. Kammlott, J. Appl. Phys. **43**, 2857 (1972).
[82]Yu. A. Golubev, L. M. Kogan, V. I. Petrov, and V. I. Rubisova, Elektron. Tekh. Ser. 2 (Electronic technology), No. 6(132), 51 (1979).
[83]H. C. Casey and J. S. Jauson. J. Appl. Phys. **42**, 2774 (1971).
[84]Yu. A. Golubev, V. V. Evstropov, V. N. Kalinin, V. P. Lejnin, and V. I. Petrov, In: Electron Microscopy (1978): Proc. 9th Intern. Congress of Electron Microscopy, Toronto, V. 1, 142 (1978).
[85]É. Yu. Barinova, V. I. Kishevskaya, Yu. A. Golubev, N. I. Kovyreva, L. M. Kogan, V. I. Petrov, and A. E. Yunovich, Fiz. Tekh. Poluprovod. **13**, 478 (1979) [Sov. Phys. Semicond. **13**, 282 (1979)].
[86]V. A. Brzhezinskiĭ, Yu. A. Golubev, and V. I. Petrov, Izv. Akad. Nauk SSSR, Ser. Fiz. **41**, 2319 (1977) [Bull. Acad. Sci. USSR Phys. Ser. **41** (11), 76 (1977)].
[87]C. Michel, J. Electrochem. Soc. **122**, 678 (1975).
[88]T J. Hayes, A. Rasul, and S. M. Davidson, J. Electron. Mater. **5**, 351 (1976).
[89]J. M. Titchmarsh, G. R. Booker, W. Harding, and D. R. Wight, J. Mater. Sci. **12**, 341 (1977).
[90]D. B. Darby and G. R. Booker, *ibid.*, 1827.
[91]H. Menniger, G. Voight, H. Raidt, H. Fabic, and J. Maege, Phys. Status Solidi **A48**, 407 (1978).
[92]S. M. Davidson, G. R. Iqbal, and D. C. Northrop, *ibid.* 29, 571 (1975).
[93]A. Rasul and S. M. Davidson, In: Ref. 58, No. 33a, 306 (1977).
[94]S. M. Davidson and A. Rasul, In: SEM 1977/1. Chicago, Il.: IITRI, 1977, V. 1, p. 225.
[95]C. A. Dimitriadis, E. Huang, and S. M. Davidson, Solid-State Electron. **21**, 1419 (1978).
[96]M. Boulou and C. Schiller, J. Microsc. et Spectrosc. Electr. **6**, 39 (1981).
[97]K. Lohnert and E. Kubalek, In: Ref. 23b, V. 2, p. 419.
[98]T. I. Ol'khovikova, A. P. Vidanov, G. N. Safonova, and F. R. Khashimov, Fiz. Tverd. Tela (Leningrad) **16**, 2813 (1974) [Sov. Phys. Solid State **16**, 1831 (1974)].
[99]G. B. Stringfellow, T. R. Cass, and R. A. Burmeister, J. Electron. Mater. **6**, 295 (1977).
[100]G. Oelgart, H. Haefner, R. Reulke, and F. Joachim, Phys. Status Solidi **A71**, 89 (1982).
[101]A. Yu. Malinin, O. B. Nevskii, M. S. Minazhdinov, A. P. Vidanov, and V. M. Mikhaelyan, Fiz. Tekh. Poluprovod. **13**, 1617 (1979) [Sov. Phys. Semicond. **13**, 941 (1979)].
[102]V. I. Petrov, Yu. A. Golubev, L. M. Kogan, and V. A. Rubisova, Elektron. Tekh. (Electronic Technology), Ser. 2, No. 4 (122), 27 (1978).
[103]Yu. P. Andreev, E. S. Dobrynina, V. N. Mel'nikova, V. I. Petrov, and V. I. Rubisova, Izv. Akad. Nauk SSSR, Ser. Fiz. **46**, 2394 (1982) [Bull. Acad. Sci. USSR, Phys. Ser. **46** (12), 118 (1982)].
[104]E. S. Dobrynina, V. N. Melnikova, and V. I. Petrov, In: Ref. 23b, V. 2, p. 415.
[105]G. B. Stringfellow and D. Kerps, Solid-State Electron. **18**, 1019 (1975).
[106]E. S. Dobrynina and V. I. Petrov, In: Electron Microscopy–1980; Proc. 7th European Congress of Electron Microscopy, The Haague, 1980 V. 3, p. 12.
[107]H. Hafner, H. Morawetz, and G. Oelgart, Phys. Status Solidi Ser. **A63**, 495 (1981).
[108]E. S. Dobrynina and V. I. Petrov, In: Electron Microscopy–1984: Proc. 8th European Congress of Electron Microscopy. Budapest, 1984, V. 2, p. 993; Izv. Akad. Nauk SSSR, Ser. Fiz. **48**, 2366 (1984) [Bull. Acad. Sci. USSR. Phys. Ser. **48** (12), 71 (1984)].
[109]A. P. Vostrova, E. S. Dobrynina, and V. I. Petrov, Fiz. Tekh. Poluprovodn. **18**, 275 (1984) [Sov. Phys. Semicond. **18**, 170 (1984)].
[110]M. K. Antoshin, G. V. Spivak, and A. E. Yunovich, Fiz. Tekh. Poluprovodn. **6**, 2123 (1984) [Sov. Phys. Semicond. **6**, 1803 (1973)].
[111]H. C. Marciniak and D. B. Wittry, J. Appl. Phys. **46**, 4823 (1975).
[112]Yu. P. Andreev, E. S. Dobrynina, V. I. Petrov, and A. V. Rubisova, Fiz. Tekh. Poluprovodn. **15**, 26 (1981) [Sov. Phys. Semicond. **15**, 15 (1981)].
[113]R. Stegmann, B. Kloth, and G. Oelgart, Phys. Status Solidi **A70**, 423 (1982).
[114]E. N. Vidgorovich, A. V. Lukichev, and A. P. Vidanov, Elektron. Tekh. (Electronic Technology), Ser. Materialy (Materials), No. 12, 89 (1977).
[115]A. P. Vidanov, T. I. Ol'khovikova, E. B. Sokolov, and F. R. Khashimov, *ibid.* No. 5, 49 (1978).
[116]G. Voigt, H. Raidt, H. Peibst, H. Menniger, and L. Hildish, Phys. Status Solidi **A36**, 173 (1976).
[117]H. Raidt, G. Kastner, H. Menninger, and G. Voigt, *ibid.* **43**, 167 (1977).
[118]V. N. Bessolov, E. S. Dobrynina, V. I. Petrov, and Yu. P. Yakovlev, Fiz. Tekh. Poluprovodn. **16**, 738 (1982) [Sov. Phys. Semicond. **16**, 476 (1982)].
[119]M. L. Vodovozova, E. S. Dobrynina, L. M. Kogan, Yu. G. Kozlov, V. I. Petrov, and G. V. Spivak, Fiz. Tekh. Poluprovodn. **13**, 1851 (1979) [Sov. Phys. Semicond. **13**, 1077 (1979)].
[120]J. I. Pankove and E. R. Levin, J. Appl. Phys. **46**, 1847 (1975).
[121]G. V. Saparin, S. K. Obyden, I. F. Chetverikova, M. V. Chukichev, and S. I. Popov, Vestn. Mosk. Univ. Fiz. Astronomiya No. 3, 106 (1984).
[122]G. V. Saparin, S. K. Obyden, I. F. Chetverikova, M. V. Chukichev, S. I. Popov, and S. I. Nikolaev, Poverkhnost' (The Surface) No. 5, 106 (1984).
[123]G. A. Perlovskiĭ, S. K. Obyden, G. V. Saparin, and S. I. Popov, Vestn. Mosk. Univ. Fiz. Astronomiya, No. 3, 21 (1984).
[124]G. V. Saparin, S. K. Obyden, M. V. Chukichev, and S. I. Popov, Microelectron. Eng. **1**, 179 (1983).
[125]V. G. Galstyan, A. V. Kuznetsov, V. I. Muratova, and G. V. Chaplygin, Izv. Akad. Nauk SSSR, Fiz. Ser. **44**, 1235 (1980) [Bull. Acad. Sci. USSR, Phys. Ser. **44** (6), 91 (1980)].
[126]A. V. Kuznetsov, V. G. Galstyan, V. I. Muratova, and G. V. Chaplygin, Mikroelektronika **11**, 343 (1982) [Sov. Microelectronics **11**, 214 (1982)].
[127]R. Bernard, F. Davoine, and P. Pinard, Optics **9**, 129 (1960); Optik **17**(3), 129 (1960).
[128]E. J. Korda, J. H. Pruden, and J. R. Williams, Appl. Phys. Lett. **10**, 205 (1967).
[129]A. I. Krokhina, M. K. Antoshin, and G. V. Spivak, Izv. Akad. Nauk SSSR. Ser. Fiz. **36**, 1915 (1972) [Bull. Acad. Sci. USSR, Phys. Ser. **36**, 1692 (1972)].
[130]M. D. Muir, P. R. Grand, G. H. Hubbard, and J. Mundell, In: SEM 1971, Chicago, Il, IITRI, 1971, p. 401.
[131]D. B. Holt, J. Mater. Sci. **5**, 546 (1970).
[132]J. Semo, Rev. Phys. Appl. **9**, 355 (1974).
[133]V. G. Galstyan, N. K. Morozova, V. A. Kuznetsov, A. A. Shternberg, and V. I. Muratova, Kristallografiya **25**, 829 (1980) [Sov. Phys. Crystallogr. **25**, 475 (1980)].
[134]M. Aven, J. Z. Devine, R. B. Bolon, and G. W. Ludwig, J. Appl. Phys. **43**, 4136 (1972).
[135]P. M. Williams and A. D. Yoffe, Philos. Mag. **18**, 555 (1968); Radiat. Eff. **1**, 61 (1969).
[136]A. D. Yoffe and K. J. Howlett, In: Ref. 27a, p. 301.
[137]S. Oda, K. Akagi, H. Kukimoto, and T. Nakayama, J. Lumin. **16**, 323

(1978).
[138]K. Akagi, H. Kukimoto, and T. Nakayama, *ibid.* **17**, 237 (1978).
[139]S. Datta, B. G. Yacoby, and D. B.Holt, J. Mater. Sci. **12**, 2411 (1977).
[140]S. Datta, P. S. Dhillon, D. B. Holt, and C. Juhasz, In: Ref. 16a, p. 279.
[141]K. Lohnert and E. Kubalek, Beitr. elektronenmikroskop. Direktab. Oberfl. **14**, 147 (1981).
[142]C. B. Norris, C. E. Barnes, and W. Boezhold, J. Appl. Phys. **44**, 3209 (1973).
[143]L. F. Komolova, V. M. Efremenkova, and G. V. Saparin, Phys. Status Solidi **A35**, K5 (1976).
[144]G. V. Spivak, L. F. Komolova, V. M. Efremenkova, and G. V. Saparin, Izv. Akad. Nauk SSSR Ser. Fiz. **41**, 933 (1977). [Bull. Acad. Sci. USSR, Phys. Ser. **41**(5), 81 (1977)].
[145]W. Bröcker and L. Riemer, Scanning **1**, 60 (1978).
[146]O. Brummer and J. Schreiber, Krist. Tech. **7**, 683 (1972); **9**, 817 (1974); Ann. Phys. (Leipzig) **28**, 105 (1972).
[147]L. F. Komolova, G. V. Saparin, G. V. Spivak, S. K. Obyden, and G. Kh. Talat, Izv. Akad. Nauk SSSR, Ser. Fiz. **41**, 880 (1977) [Bull. Acad. Sci. USSR Phys. Ser. **41** (5), 37 (1977)].
[148]L. N. Borovich, A. V. Dudenkova, Yu. M. Popov, G. Kh. Talat, L. F. Komolova, G. V. Saparin, and G. V. Spivak, Kvantovaya elektron (Moscow) **4**, 58 (1977) [Sov. J. Quantum Electron. **7**, 30 (1977)].
[149]P. A. Gashin, L. F. Komolova, G. V. Saparin, A. V. Simashkevich, and D. A. Sherban, Izv. Akad. Nauk SSSR Ser. Fiz. **40**, 2005 (1976) [Bull. Acad. Sci. USSR, Phys. Ser. **40** (9), 202 (1976)].
[150]M. K. Antoshin, I. V. Karpenko, O. I. Koval, M. M. Koltan, V. I. Petrov, and M. A. Stepovich, Izv. Akad. Nauk SSSR Ser. Fiz. **44**, 1290 (1980) [Bull. Acad. Sci. USSR, Phys. Ser. **44** (6), 138 (1980)].
[151]G. V. Spivak, G. V. Saparin, M. K. Antoshin, V. M. Stuchebnikov, and A. E. Yunovich, Fiz. Tekh. Poluprovodn. **2**, 1791 (1968) [Sov. Phys. Semicond. **2**, 1492 (1969)]; Izv. Akad. Nauk SSSR Ser. Fiz. **34**, 1422 (1970) [Bull. Acad. Sci. USSR, Phys. Ser. **34**, 1327 (1970)].
[152]M. K. Antoshin, L. V. Epifanova, and G. V. Spivak, Fiz. Tekh. Poluprovodn. **12**, 706 (1978) [Sov. Phys. Semicond. **12**, 411 (1978)].
[153]A. V. Govorkov and L. V. Druzhinina, Izv. Akad. Nauk SSSR, Ser. Fiz. **41**, 987 (1977) [Bull. Acad. Sci. USSR Phys. Ser. **41** (5), 128 (1977)].
[154]V. I. Petrov, V. A. Prokhorov, V. A. Strakhov, and N. G. Yaremenko, *ibid.* **48**, 1739 (1984) [Engl. transl. **48**, 89 (1984)].
[155]V. I. Petrov, V. A. Prokhorov, O. V. Rychkova, V. A. Strakhov, A. E. Yunovich, and N. G. Yaremenko, *ibid.* **48**, 2404 (1984) [Engl. transl. **48**, 107 (1984)].
[156]M. K. Antoshin, L. V. Epifanova, G. V. Spivak, Yu. V. Zaikin, and Yu. A. Zarifyantz, Fiz. Tekh. Poluprovodn. **12**, 1188 (1978) [Sov. Phys. Semicond. **12**, 705 (1978)].
[157]V. I. Petrov, V. A. Prokhorov, and A. E. Yunovich, Fiz. Tekh. Poluprovodn. **18**, 484 (1984) [Sov. Phys. Semicond. **18**, 300 (1984)].

Translated by A. Petelin